SLAC-PUB-10541
JULY, 2004

ARTIFACTS IN SECONDARY ELECTRON EMISSION YIELD MEASUREMENTS*

Robert E. Kirby, Stanford Linear Accelerator Center, Stanford, CA 94309, USA

Abstract

Measurement of secondary electron yields and electron energy distributions appears straightforward – simple equipment, simple electronics, easy-to-acquire data, at least in a laboratory setting. Unfortunately, the low secondary electron energy (2-5 eV) and the extreme sensitivity of the yield to surface condition and surrounding environment make the measurement details anything but simple. These problems affect the accuracy and interpretation of the experimental results, often in a subtle way. Most troublesome is the production of unwanted (and unexpected) secondary electrons from within the electron sources and detectors, and tertiary electrons from the surrounding vacuum chamber environment. In addition, the sample surface condition can change during measurement, for example, through electron damage or enhanced oxidation/carburization. Electron source, analyzer, and sample effects will be discussed with examples for oxidized Al, niobium, graphite, gold and, also, TiN coatings.

INTRODUCTION

Although air-oxidized Ti metal coatings were used for electron multipactor suppression as early as 1962 [1], it appears that the first use of the more chemically-stable compound, TiN, was on alumina ceramic klystron windows in 1974 [2]. TiN continues to be used widely today to coat beam chambers (particularly Al) and high-rf field components. Other coatings have been evaluated and found successful as well, e.g., Cr_2O_3 for ceramics [3] and TiZrV non-evaporable getter for metals [4].

The general features of secondary electron emission are well understood [5]. Primary electrons impact the surface and either reflect elastically or suffer energy loss through a variety of channels: phonon and plasmon-generating loss, ionization of atoms, free-electron scattering, surface state capture, interband transition, etc.. The electrons generated by these inelastic processes are referred to as “true secondary” while re-emitted primary electrons that suffer loss are classed as “re-diffused” primaries (Fig. 1). Most secondaries are of very low energy (2-5 eV), a result of multiple collisions, and must be within a free path of the surface (1-3 nm in metals, ~100 nm in dielectrics) in order to escape into vacuum. It is this long free path in insulators, where the loss mechanism is mostly through defect scattering, that is responsible for their high secondary yield. Secondary electron yields (SEY) over 80 have been measured in natural diamond[6].

*Work supported by the U.S. Department of Energy under contract number DE-AC03-76SF00515 (SLAC).

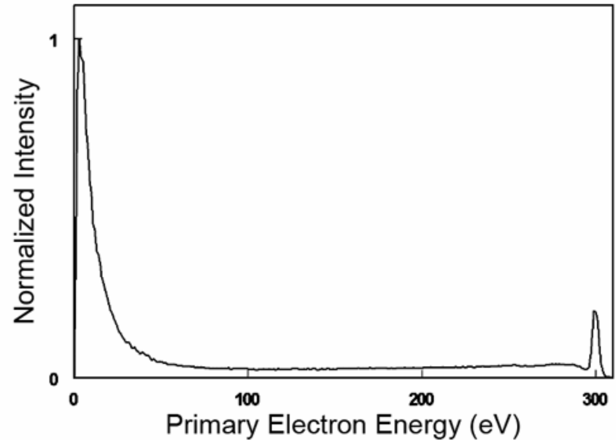

Figure 1: Secondary electron energy distribution, corrected for cylindrical mirror analyzer transmission, from TiN-coated Al beam chamber extrusion material. True secondaries (0-40eV) occupy ~ 60% area, re-diffused (40-295eV) ~ 35% area and elastics (295-305eV) ~ 5% area.

The secondary electron production process is shown schematically [7] in Fig. 2, which illustrates the crucial role of re-diffused primaries in creating multiple secondaries as they “rattle around” in the solid, but stay near the surface. That Fig. 2 represents topographic reality is shown in Fig. 3, an atomic force microscope image of extruded Al alloy beam chamber material.

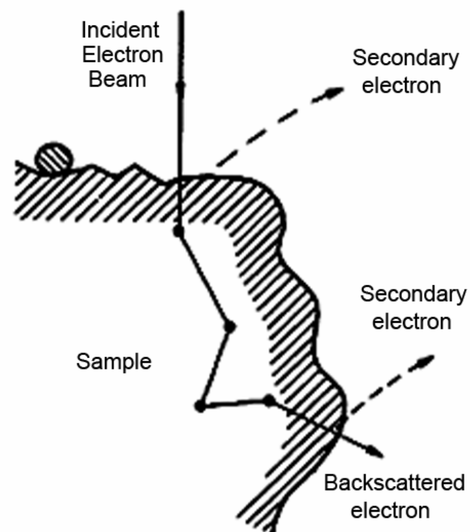

Figure 2: Schematic drawing [7] of primary electron path (solid line) in sample. Low energy (“true”) secondaries can escape into the vacuum from the shaded surface layer.

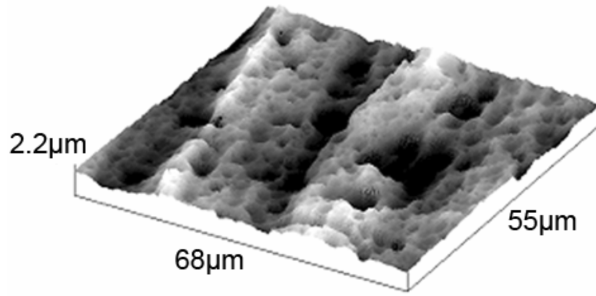

Figure 3: Atomic force microscope topographic image of extruded Al-6063 alloy beam chamber material. Grooves are parallel to the extrusion direction.

The principal mechanism for SEY reduction in "perfect" crystals is electron-electron scattering. Therefore, in perfect insulators, there is effectively no loss mechanism other than lattice vibrations and inter-band transitions. In technical materials, however, defect scattering and surface layers have a major effect on SEY reduction. Such surfaces might be characterized as an agglomeration of semiconducting oxides and carbides, "glued" down with unpolymerized hydrorcarbons and water.

In the course of measuring secondary electron yields from various materials [3, 8-10}, using several methods, we have noticed and studied some data variations caused by 1)secondary "primary" electrons generated inside the electron source, 2)tertiary electrons generated from chamber walls and components, 3)tertiary electrons generated from the structure of the energy distribution measuring spectrometer, 4)sample surface modification by primary electrons and, 5)substrate backscatter contribution to the yield of thin overlayers. The presence of these effects is generally recognizable and preventable.

EXPERIMENTAL DETAILS

Yields are generally measured either by monitoring the sample current or by collecting the scattered primary and secondary emission with a retarding field analyzer (RFA) or biased Faraday cup. Each technique has defects which can contribute to potential misinterpretations of the data.

The simplest sample current method, the retarding potential (RP), consists in fixing the primary electron gun potential and then determining the final electron energy at the sample by voltage bias retardation. Fig. 4 shows the layout of this technique where the yield δ is determined from the sample and primary currents as

$$\delta = 1 - I_T/I_P$$

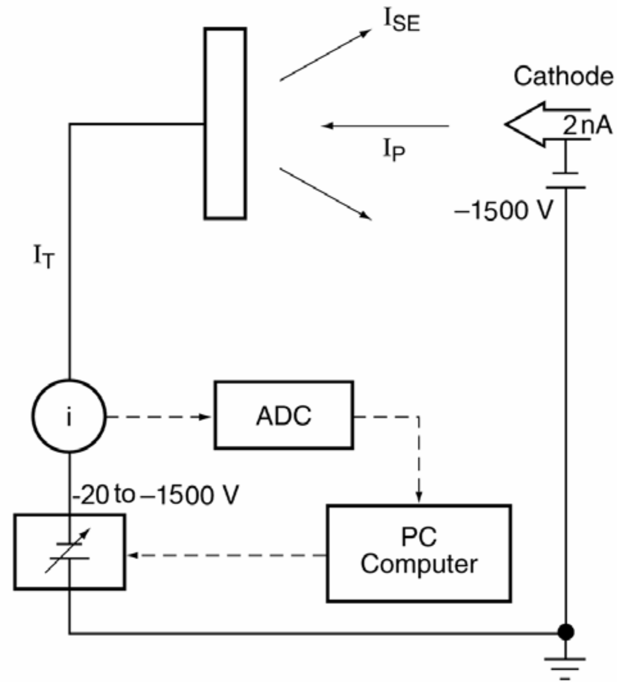

Figure 4: Retarding potential (RP) measurement layout. ADC= analog-to-digital converter. The "target" or sample current, I_T, is measured with a high voltage-isolated picoammeter.

The key ingredient of this technique is a stable low-leakage high voltage (up to cathode potential) isolatable sample current-measuring picoammeter. To minimize modification of the sample surface by the primary beam, the primary current must be on the order of a nanoamp, with data collection of several minutes per curve. That implies a desired sample leakage of 1pA or less. Retard voltage scanning begins with a small bias on the sample of –20V in order to prevent tertiary electrons from the chamber returning to the sample (this point will be discussed in detail later). Disadvantages of the RP method include no collection of the elastically-reflected beam and no non-normal incidence measurement where a retarding field becomes a deflecting field and moves the beam off the sample at high retardation voltage (low energy). Advantages are simple equipment and no space charge limit in the electron gun to achieve low (<200 eV) incident energy and, of course, stable primary beam current.

If an angle of incidence other than normal is needed, the sample and the volume surrounding it must be in a field-free configuration (no retardation). The setup of Fig. 4 could be used, if the electron gun is capable of operating down to the lowest energy needed (which must be >200eV with space charge-limited unipotential guns, more on this later) and the behavior of the beam current vs. cathode potential is known (i.e., measured), so that the I_P is known throughout the primary energy range. Further, the sample cannot be biased to reject chamber tertiaries because of primary beam deflection. Elastically scattered

primaries can strike nearby surfaces and create copious tertiaries that can return to the sample. This problem can be somewhat controlled by placing a gridded collector behind the sample that passes and traps the forward-scattered primary electron beam.

Neither of these RP techniques can be used to measure the elastic backscatter coefficient nor the energy distribution curve (EDC) of the secondary electron spectrum. Commercial gridded (e.g., retarding potential) or differential (e.g., cylindrical mirror) analyzers used for these purposes usually collect only a portion of the 2π-steradian emission. In addition, the emission spectrum itself is not angularly uniform, even for polycrystalline samples, because the elastic backscatter is peaked sharply about the normal while the true secondaries are emitted in a cosine distribution. Therefore, a differential measurement is sure to get the relative population of each type wrong, at all angles.

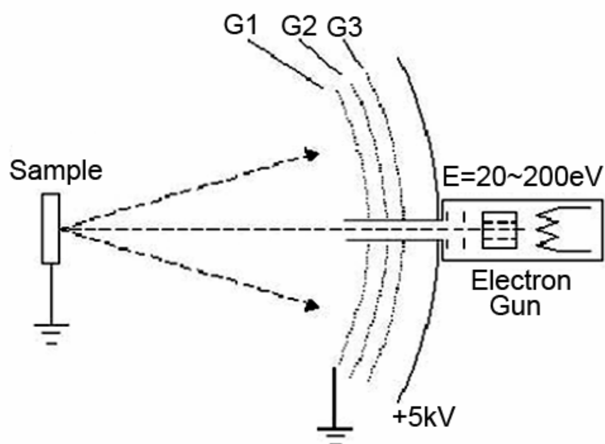

Figure 5: Retarding field analyzer schematic, showing the penetration of the gun drift tube through the grids and collector. G2 is the retarding grid for EDC measurements. G1 establishes a field-free region; G3 is an electrostatic shield grid.

A typical 120° acceptance angle RFA is shown in Fig. 5. A serious defect in this type of analyzer is the creation of tertiary electrons on the gun collimator, grid housing and grids. Some of these return to the sample while others, under some grid biases, can penetrate and reach the collector. There is no ideal solution to these problems and a combination of techniques and well-characterized instrumentation is essential to obtaining artifact-free data, especially at low primary and secondary energies.

RESULTS AND DISCUSSION

Electron source artifacts

From our earliest SEY measurements, we noticed that tuning of the electron gun focus lens could, in some instances, affect the shape of the SEY curve. An example of this effect is shown in Fig. 6 for sputter-cleaned Nb. The location of the unexpected "dip, at approximately 700eV primary energy, shifted correspondingly with electron gun focus lens setting.

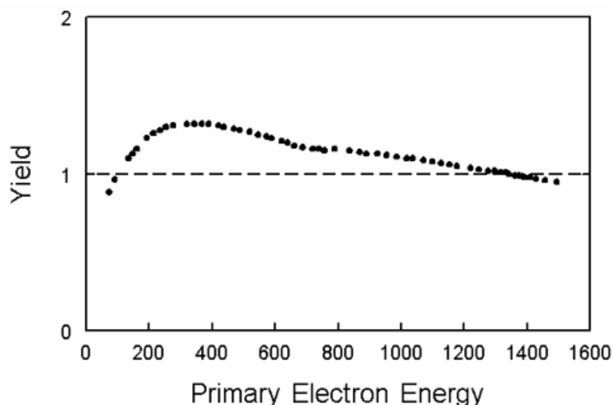

Figure 6: RP SEY data from clean Nb. Fixed cathode potential = -1500V.

The cause of the dip is easier to understand if the SEY of Fig. 6 is presented as target current vs. sample retard voltage (gun cathode at –1500V). Included with this plot, in Fig. 7, is a dashed line showing the expected SEY shape below –800V retard. The extra sample current bears a resemblance to a second, additional sample current yield.

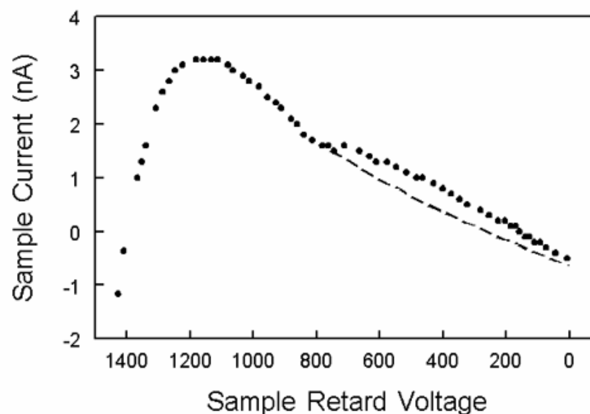

Figure 7: SEY of Fig. 6, displayed as the original sample current data. The dashed line is the expected shape of the current, in the absence of the dip and extra current.

A measurement of the primary electron gun beam, with a Faraday cup (Fig. 8), found a halo of electrons present. Our energy analyzer confirmed the presence of a small elastically-scattered peak at 950eV, in addition to the main component at 1500eV. This current slice across the diameter gave a peak Faraday cup current of 0.6%. Integration of the entire halo current yields ≈12.5% of the main beam. We scaled the current of Fig 7 by 0.1 and shifted it by +550V (the focus lens potential relative to the cathode potential) to give the approximate contribution of the focus lens "primary" secondary electrons, Fig. 9.

When this contribution is subtracted from the sample data, the dip is reduced and the current slope is corrected.

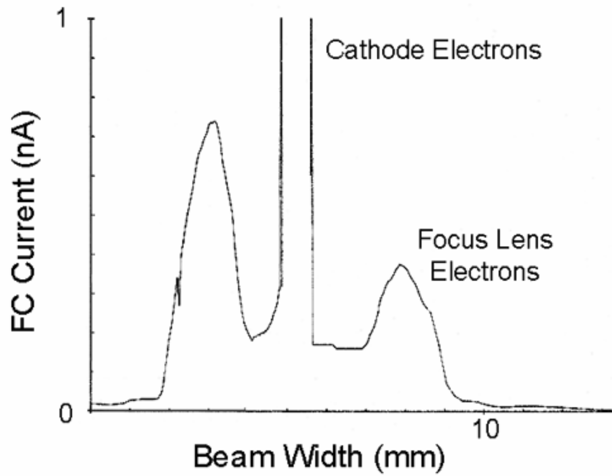

Figure 8: Faraday cup (0.25 mm diameter circular aperture) measurement of current leaving the electron gun used to collect Fig. 7. The asymmetric "halo" is due to secondary electrons generated from the focus electrode by cathode electrons.

Finding which gun element was responsible, in this case, was easy because of the simplicity of the gun element structure (Fig. 10). The focus lens was the only element not at cathode or ground potential. This type of gun derives its voltages from a single high-voltage source and a resistive divider ("unipotential"). This is the classic gun structure of the monochrome television, whose principle defect for use as a primary electron source is severe space charge at low cathode potentials (<200eV).

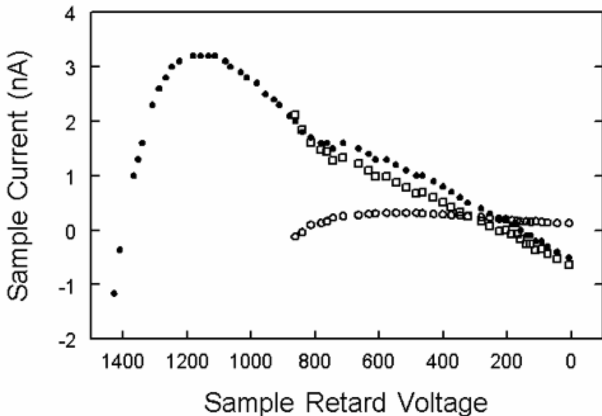

Figure 9: Sample current difference (open squares) after subtraction of scaled and shifted focus lens "primary" secondary current (open circles) from the original data (dots).

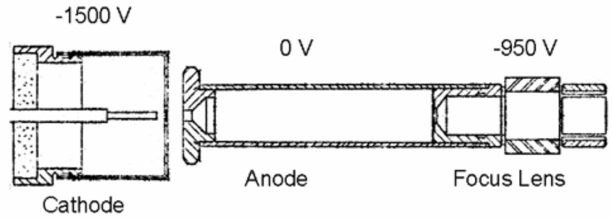

Figure 10: Commercial [11] unipotential electron gun used to collect data of Fig. 6 in RP mode. The downstream element of the focus lens ("-950V") is the source of the secondary electrons that strike the sample. Voltage labels are relative to ground.

More sophisticated gun structures have been designed and manufactured that overcome the cathode space charge limitation directly by using a combination of fixed high voltage cathode potential followed by a retarding "zoom" lens that decelerates the beam to final energy near the gun downstream end. The beam then drifts to the sample. Such guns (Fig. 11) are capable of operating down to less than 10eV. Primary electron energy is changed by varying the cathode potential (VC).

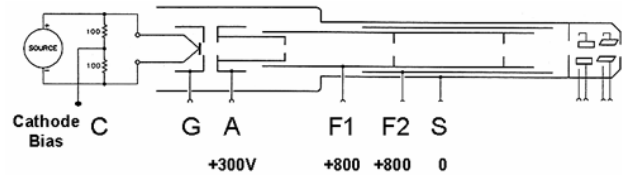

Figure 11: Complex electron gun design incorporating fixed cathode/anode potentials for the accelerating and beam-forming sections (cathode C, grid G, anode A, first focus F1) in order to overcome cathode space charge [12].

As in the unipotential gun, improper setting of gun potentials leads to secondaries being generated on elements (probably at aperture edges). Some of these escape the gun and form one or more primary "secondary" sources. Examples of this are shown in Fig. 12 and 13 for mis-set anode and focus lens 1 potentials.

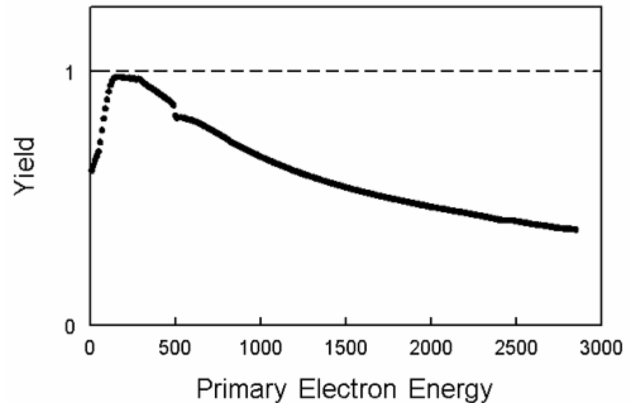

Figure 12: VC SEY data from graphite [13], sputtered-cleaned, with anode potential mis-tuned to cause secondary electron generation from the anode aperture A of the gun.

The feature produced in Fig. 13 actually involves two gun elements, the focus 1 aperture, (where secondaries are generated) and the grounded gun collimator, from which these secondaries scatter on their way out of the gun. This scatter effect occurs when the lens focusing strength is low and switches off when the strength increases. Then the secondaries are either blocked from leaving the gun by striking a plate or all of the cathode primaries pass through the aperture without striking it. Hence, the extra electrons in the primary beam switch on at 10eV and switch off at 80eV.

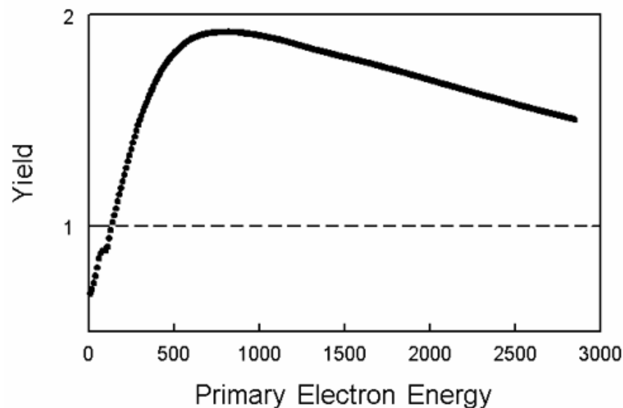

Figure 13: VC SEY data from Au(110), sputter-cleaned. Focus 1 is mistuned to generate secondaries from its aperture.

Tertiary electron production

All but the lowest energy secondary and elastically-reflected electrons leaving the sample and striking nearby components and the chamber wall are capable of generating tertiary electrons, some of which may return to the sample. The easiest way to prevent these tertiaries from hitting the sample is to apply a small negative bias to the sample. The effect of tertiaries and bias is shown in Fig. 14. Tertiaries reduce the total current leaving the sample surface because of their low energy ($\delta<1$).

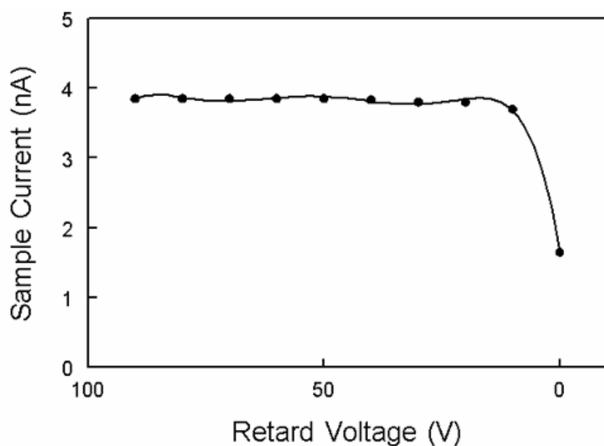

Figure 14: RP data from sputter-cleaned Al covered with native oxide. At –10V retard most of the tertiary electrons from the surrounding chamber are rejected.

In the Experimental Details section, mention was made of this tertiary-rejecting bias (Fig. 4). SEY data taken by both methods, RP and VC, are plotted in Figure 15. In the RP case, the first -20V of retard data is discarded; in the VC case, the bias on the sample is a constant –20V. The agreement is generally good. The disagreement at lowest energy on this specific sample is possibly due to conditioning of the delicate native oxide in the RP measurement, because the lowest energy primaries are deflected over to an unconditioned portion of the sample, giving a slightly higher yield.

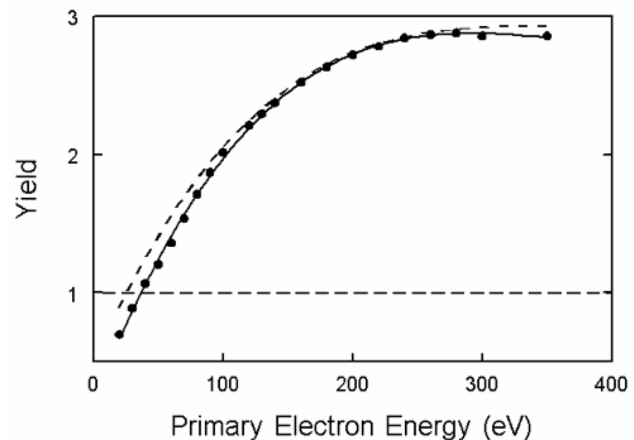

Figure 15: SEYs from sputter-cleaned Al with a native oxide. Displayed are an RP (solid line) and VC (dashed) SEY of the same surface area.

Measuring the SEY with an RFA does not avoid the tertiary problem. Elastic and secondary electrons from the sample strike the RFA and generate tertiaries on the grid housing, gun collimator and grids. Depending on grid biasing some of these will make it to the RFA collector while some return to the sample. Figure 16 is RFA data from Cross [14] showing the creation of teriaries on the inner grid and on the collimator. In the RFA, tertiaries are generated at the gun collimator (V=0), at the field-free inner grid (closest to the sample, also usually V=0) and on the negative retarding grid (when collecting an EDC). For the figure data, the retarding grids were biased a few volts positive to increase collection of the tertiaries and separate the collimator tertiary electrons from the inner grid tertiaries. Tertiaries make their way to the collector through grid penetration at high (typically, several kV) RFA collector biases, or through direct generation on the negative retarding grid. Electrons generated from the sample can be distinguished (except for elastics) from those generated elsewhere in the system by applying a small negative bias to the sample. Sample secondaries will shift to higher energy in the EDC spectrum, by the sample bias amount. Characterizing the behavior of the RFA , particularly at low energy, is essential to sensible interpretation of results at low energy. Many discussions of these problems can be found in 1970s publications describing low energy electron diffraction equipment.

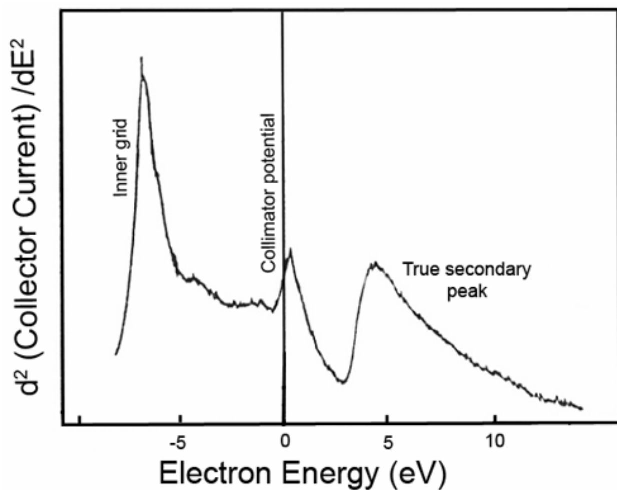

Figure16: Tertiary electron spectrum generated inside a retarding field analyzer from its gun collimator and the grid closest to the sample[14]. The sample has been biased -3V to separate the sample secondaries from the RFA tertiaries.

Surface modification by incident electrons

These changes are loosely grouped as "electron conditioning" and include desorption, carburization, oxidation, and damage. Desorption of surface gases and the carburization of carbon-containing molecules on the surface have a dramatic effect on SEY. Studies have shown that H, CO, CO2 and CH4 are electron-desorbed from Al extrusion, with H and CO2 having an initial rate of 1 molecule/electron [15]. The chemical state of the carbon influences the SEY through the emission transmission probability. The probability is increased by up to 50% for water and aromatic hydrocarbons and reduced by up to 50% for polymerized and elemental carbon [16]. The mechanism is the hybridization of molecular surface states with conduction band electrons. The transmission of secondaries is controlled through the elastic/inelastic crossection at the surface barrier.

Oxidation of surface metal atoms is encouraged by the ability of the electron beam to dissociate water and create OH- [17]. Perfect oxides have high yields but defective oxides, such as are produced by electron impact, can reduce the SEY. These sub-oxides are semiconductors that contribute both electron-electron and defect-electron scattering, thus reducing the SEY. TiO_2 is the prototype metal oxide surface, whose defect structure has been studied extensively [18,19].

Finally, an unusual source of surface CO was found at SLAC in 1968 [20]. Under electron bombardment, bulk CO was observed to move up the grain boundaries to the surface of Al covered by a thin layer of γ-Al_2O_3. This was confirmed by the use of CO^{18} adsorption from the gas phase. Thus, in some cases, the bulk can be an important source of carbon for SEY reduction during the conditioning process.

Substrate backscatter effect

SEY enhancement via primary electron backscatter is not normally a problem unless the SEY-suppressing overcoating is very thin, <1.5 nm in the case of TiN-coated klystron windows, for example. Monte Carlo simulation (Fig 17) of the penetration of 500eV primary electrons into TiN, at normal incidence, shows that the range is 2-3 nm.

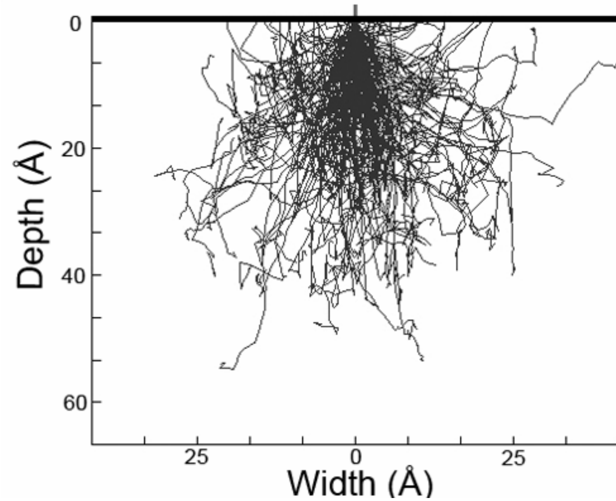

Figure 17: Monte Carlo simulation of the penetration of a 500eV primary electron beam into TiN [21].

This means that backscattered primaries from the substrate will penetrate the overlayer on return to the surface, thereby enhancing the SEY. Fig. 18 illustrates this effect for TiN overlayers on Nb. The difference in yields, based on TiN thickness, increases from 50eV up to 750eV or so where the primary electron range is large compared to overlayer thickness (50 nm at 3keV). This effect is important in cases, such as the coating of klystron windows where the overlayer thickness must be effective for SEY reduction but not so thick as to cause ohmic heating in operation.

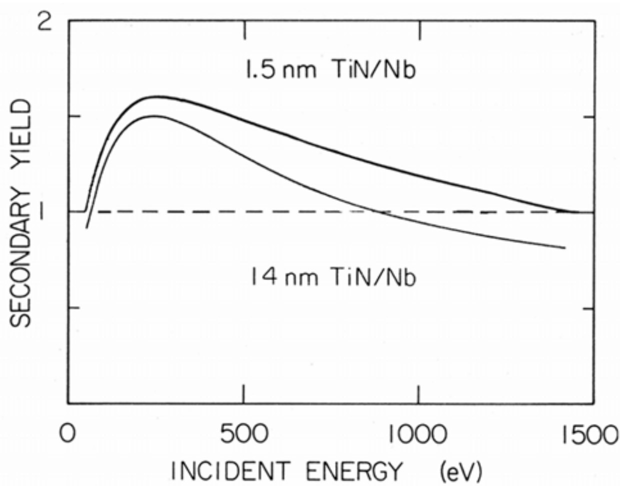

Figure 18: RP SEY from TiN (two different thicknesses) deposited on bulk polished Nb substrates. The films were deposited and measured without atmospheric exposure.

Very low primary energy and elastic reflection

At this point, it should be obvious that low electron energy is a difficult region of SEY and EDC spectra to measure unambiguously. The elastic reflection coefficient itself at low energy is dependant on a number of processes. The most obvious of these is Bragg diffraction from a surface periodic structure. Although beam chambers are composed of polycrystalline metals, the overall surface frequently has a crystalline texture. For example, recently we measured, with x-ray diffraction, a <111> texture on as diamond-machined OFE Class 1 copper. Enhancements to the elastic reflection coefficient, however, are limited to a narrow energy range determined by a combination of the Bragg condition and multiple scattering effects. Examples of such reflections are shown in Figures 19 and 20.

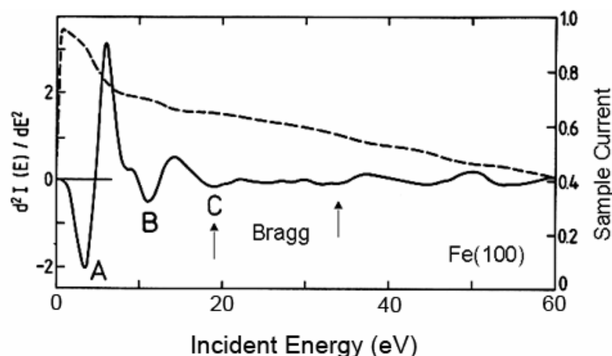

Figure 19: Sample absorbed current for Fe(100), raw data (dashed) and differentiated result that shows the location of Bragg reflections [22]. Other features are due to empty conduction band states.

Figure 19 is a plot of experimentally-measured absorbed (i.e., 1-yield) current for single-crystal Fe(100). The absorbed current rises close to one until the beam is cut off by the contact potential difference between cathode and sample. Despite the fact that this was a verified periodic surface, the Bragg reflections have rather little effect on the absorbed current. The absorbed current is determined by the availability of empty states above the conduction band of Fe(100).

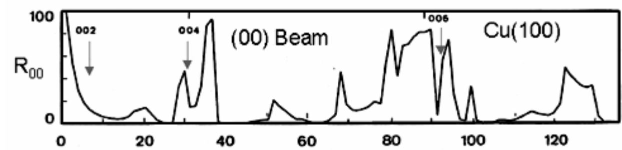

Figure 20: Bragg reflections for Cu(100), as theoretically predicted [23]. In this case, a strong reflection is predicted at a few eV primary energy for this periodic surface.

Figure 20 is a theoretical prediction for the Bragg behavior of Cu(100). In this case, there is a reflection near zero primary energy. Not included, of course, is the inelastic behavior of the current, which may be substantial, as it is for Fe(100). In general, technical surfaces are not single crystal, are covered with defects (surface states) and, at least, native oxides, adventitious carbon and water. Accordingly, inelastic processes (e.g., intra/interband and Auger transitions) are the dominant mechanism expected to govern the secondary yield at low primary energy.

Returning to further discuss the contact potential cutoff identified in Figure 19, this feature should (and does) have the Maxwell-Boltzmann thermal energy distribution of the hot cathode. Figure 21 is a plot of several materials exhibiting the contact potential cutoff.

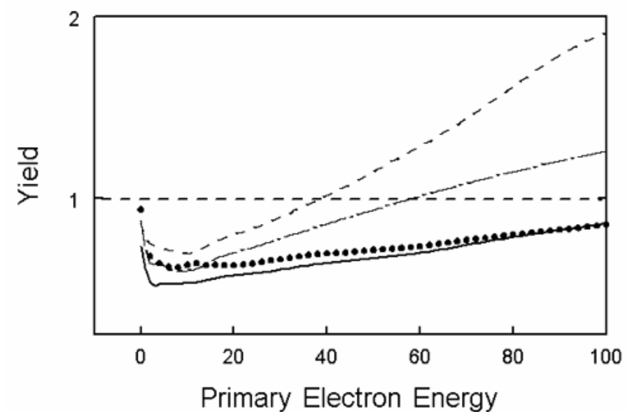

Figure 21: VC SEY data from TiN (–·–), Au(110)(•••), oxidized Al(---) and graphite(—). TiN was as-deposited and air-exposed, other surfaces were sputter-cleaned.

Three of the samples were ion-bombarded, but not annealed, hence no Bragg features are possible. At zero energy, the sharp rise is due to the mirror reflection of the incoming beam by the contact potential difference between cathode and surface. The zero of energy is the vacuum level of the sample. Note that all four of these

yields are converging on 0.3-0.5. Clean surface, disordered, no Bragg reflections. Also the slope extends out smoothly to 100 eV and more. Why not zero yield at zero energy? There should be a continuum of bulk and surface states available for full absorption. The literature of absorbed current spectroscopy shows that the zero energy absorption varies widely depending on band structure and surface states. Ion sputtered, but not annealed, surfaces are covered in defects [19], hence the yield for such surfaces should be low.

FINAL COMMENT

The current interest in the interactions of low energy electrons with surfaces, particularly with the elastic coefficient, echos back to a period of research, both theoretical [24]and experimental [25,26], on the behavior of low energy secondary electron emission from ordered and disordered crystal surfaces. Details of the inelastic electron spectrum may be found in publications of that era.

ACKNOWLEDGEMENTS

Many colleagues have contributed to SLAC's SEY measurement program since 1975, particularly Ed Garwin who began the program and maintains a keen interest in its development. Their affiliations at the time of their contributions are listed: Ed Garwin, Frank King, Earl Hoyt, Frederic Le Pimpec, Mauro Pivi, and Ali-Reza Nyaiesh, SLAC; Takashi Momose, Tohoku University; Osamu Aita, Osaka Prefecture University; Erhard Kisker, KFA, Julich; and Pilar Prieto, Universidad Autonoma Madrid.

REFERENCES

1. R. C. Talcott, I.R.E. Trans. On Electron Devices ED-9 (1962) 405.
2. K.M Welch, SLAC-PUB-1472 (1974).
3. R.E. Kirby, E.L. Garwin, F.K. King and A.R. Nyaiesh, J.Appl.Phys.62 (1987) 1400.
4. B. Henrist, N. Hilleret, C. Scheuerlein, and M. Taborelli, Applied Surf. Sci. 172 (2001) 95.
5. H. Seiler, J. Appl. Phys. 54 (1983) R1.
6. A. Shih, J. Yater, C. Hor and R. Abrams, Applied Surf. Sci. 111 (1997) 251.
7. Electron Beam Interactions with Solids for Microscopy, Microanalysis and Microlithography: Proceedings First Pfefferkorn Conference, D.F. Kyser et al, Ed., Scanning Microscopy, Inc. (1982).
8. E.L. Garwin, F.K. King, R.E. Kirby and O. Aita, J. Appl. Phys. 61 (1987) 1145.
9. E.L. Garwin, E.W. Hoyt, R.E. Kirby and T. Momose, J. Appl. Phys 59 (1986) 3245.
10. R.E. Kirby and F.K. King. Nucl. Instr. and Meth. in Phys. Research A469 (2001) 1.
11. Varian, Inc. integral Auger electron gun, model 2611.
12. Kimball Physics, Inc., model ELG-5.
13. POCO Graphite, Inc., type AXF-5Q.
14. J.A. Cross, J. Phys. D6 (1973) 622.
15. M.Q. Ding and E.M. Williams, Vacuum 39 (1989 463.
16. J. Halbritter, J. de Physique 45 (1984) C2.
17. I. Popova, V. Zhukov and J.T. Yates, Jr., Appl. Physics Lett. 75 (1999) 3108.
18. R. Patel, Q. Guo, I. Cocks, E.M. Williams, E. Roman and J.L. de Segovia, J. Vac. Sci. Technol. A15 (1997) 2553.
19. W. Gopel, J.A. Anderson, D. Frankel, M. Jaehnig, K. Phillips, J.A. Schafer and G. Rocker, Surf. Science 139 (1984) 333.
20. E.L. Garwin, E.W. Hoyt, M. Rabinowitz and J. Jurow, Proc. Fourth Int. Vacuum Congr., Manchester Pt.1 (1968) 131.
21. Electron Flight Simulator V.3.1 software, Small World,LLC.
22. E. Tamura, R. Feder, J. Krewer, R.E. Kirby, E. Kisker, E.L. Garwin, and F. King, Solid State Commun.55 (1985) 543.
23. G. Capart, Surf. Science 26 (1971) 429.
24. W. Moritz, H. Jagodzinski and D. Wolf, Surf. Science 77 (1978) 249.
25. R.F. Willis and N.E. Christensen, Phys. Rev. B18 (1978) 5140.
26. H.-G. Zimmer, D. Westphal, K.K. Kleinherbers and A. Goldmann, Surf. Science 146 (1984) 425.